

1-Octyl-2-(octylthio)-1H-benzimidazole as a New and Effective Corrosion Inhibitor for Carbon Steel in 1 M HCl

F. El-Hajjaji^a, I. Merimi^b, L. El Ouasif^c, M. El Ghoul^c, R. Achour^c,
B. Hammouti^b, M.E. Belghiti^a, D.S. Chauhan^{d,*} and M.A. Quraishi^d

^a *Laboratoire d'Ingénierie d'Electrochimie, Modélisation et d'Environnement (LIEME), Faculté des Sciences/Université Sidi Mohammed Ben Abdellah, Fès, Morocco*

^b *Laboratoire de Chimie Analytique Appliquée, Matériaux et Environnement (LC2AME), COSTE, Faculté des Sciences, Oujda, Morocco*

^c *Laboratoire de Chimie Organique Hétérocyclique, Université Mohammed V, Faculté des Sciences, Rabat, Morocco*

^d *Center of Research Excellence in Corrosion, Research Institute, King Fahd University of Petroleum and Minerals, Dhahran- 31261, Saudi Arabia*

Received June 24, 2017; accepted December 15, 2017

Abstract

The corrosion inhibition effect of 1-octyl-2-(octylthio)-1H-benzimidazole (T3) on mild steel in a 1 M hydrochloric acid solution was studied using weight loss measurement, potentiodynamic polarization and electrochemical impedance spectroscopy (EIS) techniques, at 308 K. This compound has exhibited a corrosion inhibition efficiency of 93% at 10^{-3} M concentration. The adsorption of this molecule onto the mild steel surface obeyed Langmuir adsorption isotherm. Potentiodynamic polarization measurements indicated that the studied compound acted as a mixed type corrosion inhibitor. EIS results showed that an increased inhibitor concentration led to an increase in the polarization resistance and decrease in the double layer capacitance.

Keywords: mild steel; corrosion inhibition; benzimidazole; electrochemical impedance spectroscopy and potentiodynamic polarization.

Introduction

Corrosion inhibitor is a chemical substance which significantly reduces the rate of metallic corrosion in a corrosive environment. Corrosion inhibitors are widely used in various fields, such as oil mining and processing, acid pickling, industrial water recycling systems, and so on [1-3], due to their low cost and ease of application. Most of the corrosion inhibitors are organic compounds containing heteroatoms, such as oxygen, nitrogen, sulfur, phosphorus, unsaturated bonds, or plain conjugated systems [3-8], which can slow down metals corrosion by adsorbing onto the metal surface, forming a protective barrier between it and the corrosive medium.

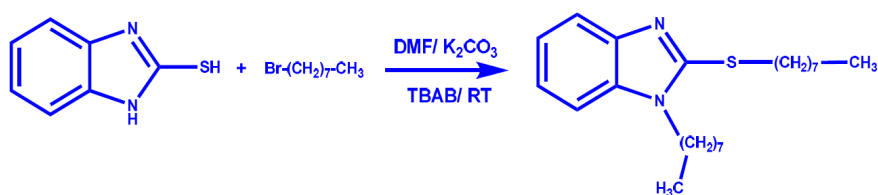
* Corresponding author. E-mail address: dschauhan.bhu@gmail.com

Benzimidazole is nitrogen containing heterocyclic aromatic organic compounds. Benzimidazole and its derivatives can adsorb onto the metallic surface, due to the presence of nitrogen atoms and aromatic rings in the molecular structure. The relationship between the structure of benzimidazole derivatives and their corrosion inhibition performance was also investigated [8-13]. Encouraging results obtained by 1-tetradecyl-2-(tetradecylthio)-1H-benzimidazole (T1) [13] with an aliphatic carbon chain (14C) incited us to prepare another analogue having an 8 carbon alkyl chain, i.e., 1-octyl-2-(octylthio)-1H-benzimidazole (T3), and to test it as a corrosion inhibitor for carbon steel in a 1 M HCl solution. The present compound (T3) had not yet been tested as a corrosion inhibitor on carbon steel in HCl. It was selected because it can readily adsorb onto the steel surface, due to a positively charged nitrogen atom; also, the long hydrocarbon chain is likely to form a hydrophobic network which can further reduce the interaction between the metal and the corrosive environment. T3 corrosion inhibition behavior was studied using potentiodynamic polarization, electrochemical impedance spectroscopy and surface analysis techniques. In addition, Monte Carlo simulation was carried out to theoretically estimate the structural aspects of T3 that are significant for corrosion inhibition behavior.

Experimental details

Inhibitor synthesis

To a solution of 2 g (133×10^{-4} mol) of 2-mercaptobenzimidazole and 80 mL of N,N-dimethylformamide was added 3.67 g (266×10^{-4} mol) of potassium carbonate, 13.3×10^{-4} mol of tetra-n-butylammonium bromide and 7.71 g (399×10^{-4} mol) of 1-bromooctane. The reaction mixture was stirred at room temperature for 24 hours. After filtration, the solvent was removed under reduced pressure. The residue was taken up in dichloromethane, filtered, and the solvent was evaporated under reduced pressure (Scheme 1).



Scheme 1. Synthesis of 1-octyl-2-(octylthio)-1H-benzimidazole (T3).

The structure of the compound was characterized by ^1H NMR, ^{13}C NMR and mass spectrometry (Fig. 1).

Thus, the ^1H NMR spectrum recorded in CDCl_3 showed a multiplet between 7.18 ppm and 7.73 ppm for the aromatic protons, a triplet at 4.06 ppm for NCH_2 , a triplet at 3.44 ppm for SCH_2 , a multiplet between 1.25 ppm and 1.81 ppm corresponding to the protons carried by the methylene groups of the hydrocarbon chain, and a triplet at 0.86 ppm for CH_3 . On the other hand, the ^{13}C NMR spectrum recorded in CDCl_3 showed a signal at 152.07 ppm for the carbon bonded to the sulfur atom, signals between 31.8 ppm and 22.61 ppm

corresponding to the carbon of the methylene groups, and signals at 14.1 ppm for CH_3 . The mass spectrum shows a molecular ion peak $[\text{MH}]^+$ at $m/z = 375$.

Yield: = 88%, ^1H NMR (CDCl_3) (δ ppm): 0.86: (t, 6H, $-\text{CH}_3$); 1.25-1.81: (m, 24H, $-\text{CH}_2$); 3.44: (t, 2H, SCH_2); 4.06: (t, 2H, NCH_2); 7.18-7.73: (m, 4H, $\text{CH}_{\text{benzene}}$). ^{13}C NMR (CDCl_3) (δ ppm): 14.1: (CH_3); 22.61-31.80: ($-\text{CH}_2$); 32.82 (SCH_2); 44.28: (NCH_2); 108.821-142.38: (CH , phenyl); 152.07: ($\text{C}=\text{N}$).

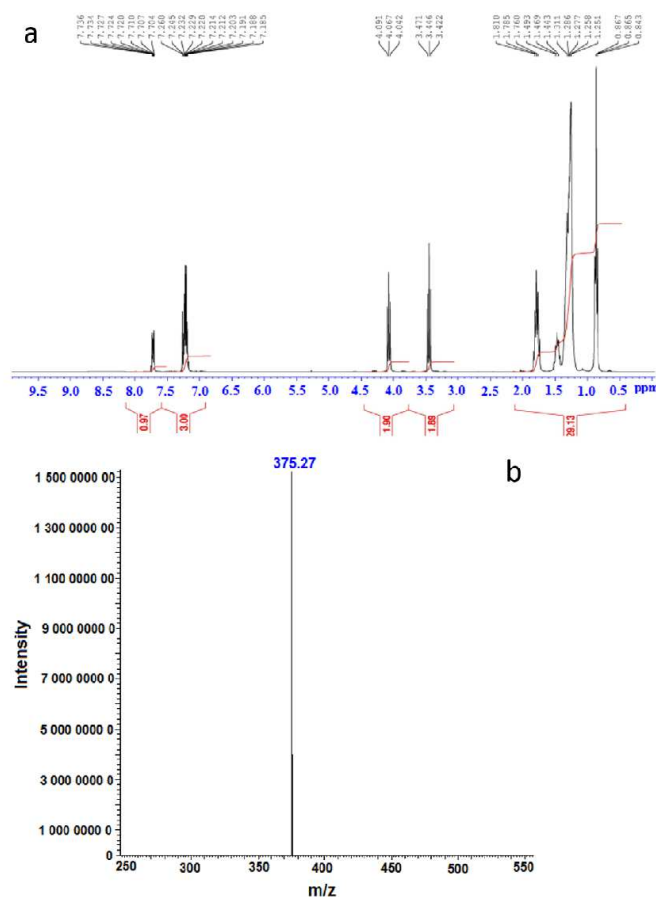


Figure 1. (a) ^1H NMR and mass spectrum (b) of 1-octyl-2-(octylthio)-1H-benzimidazole

Materials preparation

Mild steel coupons used for electrochemical measurements had a composition of 0.076% C, 0.192% Mn, 0.050% Cr, 0.026% Si, 0.012% P, 0.135% Cu, 0.023% Al, 0.05% Ni and balance Fe. The coupons were mechanically polished using emery paper of grades no. 600, 800, 1000 and 1200, thoroughly washed with deionized water, and finally degreased with acetone.

Electrochemical measurements

Potentiodynamic polarization measurements

Potentiodynamic polarization measurements were carried out in a three electrodes cell using PGZ 301 Electrochemical Analysis System. A saturated calomel electrode (SCE) was used as reference electrode, and a Pt electrode as counter electrode. The working electrode was prepared from a cylinder of steel,

and the exposed surface area was 1 cm². The cell was equipped so that the temperature during each experiment was kept constant and measurable.

The polarization curves were potentiodynamically obtained in the potential range between -0.800 V and -0.200 V at open circuit potential (OCP), with a scan rate of 1 mVs⁻¹. The working electrode was immersed in the test solution for 30 min prior to each experiment, which proved sufficient for OCP to attain a reliable stable value. The inhibition efficiencies (IE%) were calculated using the following relation:

$$IE\% = \frac{i_{corr} - i_{corr}^{inh}}{i_{corr}} \times 100 \quad (1)$$

where i_{corr} and i_{corr}^{inh} are the corrosion current densities without and with T3, respectively, determined by the extrapolation of anodic and cathodic Tafel curves to the respective corrosion potentials.

Electrochemical Impedance Spectroscopy

The impedance spectra were obtained in the frequency range of 100 kHz to 10 mHz, with 10 points per decade at the OCP, after a stabilization period. A 10 mV sine wave ac voltage was used to perturb the system. The double layer capacitance (C_{dl}) and polarization resistance (R_p) were calculated from Nyquist plots, as described elsewhere [13]. Since R_p is inversely proportional to the corrosion current, it was used to calculate the inhibition efficiency (IE%) from the following relation:

$$IE\% = \frac{R_p^{inh} - R_p}{R_p^{inh}} \times 100 \quad (2)$$

where R_p and R_p^{inh} are the polarization resistance values, without and with the inhibitor, respectively. The EIS results are analyzed using ZView software, and fitted using the appropriate equivalent circuit.

Surface morphology

The mild steel surface morphology after the polarization test in acidic solutions, in the absence and presence of optimum inhibitor concentrations, was examined by FEI QUANTA 200 scanning electron microscope (SEM).

Molecular dynamic simulations

The Monte Carlo simulation was implemented to determine the adsorbate/substrate system interaction. Metropolis Monte Carlo simulations methodology, [14] using DMol₃ codes [15-16] and an adsorption locator module [17-18] implemented in the Accelrys Materials Studio version 8.0 [19], was used to build the system (inhibitor molecule/solvent/iron). The DMol₃ geometry optimization of the inhibitor molecule in the neutral form, before putting it on the clean iron surface in an aqueous phase, was performed using B3LYP functional with DNP+ used as the basis sets for all atoms. Herein, the interaction between the Fe (111) crystal surface and the single inhibitor molecules (S_1 & S_2) was

executed in a simulation box of $35.179 \text{ \AA} \times 35.375 \text{ \AA} \times 40.266 \text{ \AA}$, with periodic boundary conditions. The crystal surface (111) was chosen for this simulation, because it is among the most stable and low energy surfaces, as reported in the literature [20]. The simulation systems were carried with a slab of 5.0 \AA thickness, a super cell of 6×6 , and a vacuum of 30 \AA along the Z-axis, with periodic boundary conditions, in order to simulate the representative part of an interface devoid of any arbitrary boundary effects. The behavior of the studied inhibitor molecules on Fe (111) was then simulated by COMPASS force field [21-22], which is an ab-initio force field that enables accurate predictions of gas-phase (structural, conformational, etc.) and condensed-phase properties (state equation, cohesive energies, interaction energies, etc.) for a broad range of organic molecules; the metal was used for geometrical optimization of all systems [21]. The liquid phase comprising one hundred water molecules was added to simulate the solvent effect, since the corrosion takes place in an acidic solution.

Results and discussion

Potentiodynamic polarization

Electrochemical parameters such as corrosion current density (I_{corr}), corrosion potential (E_{corr} vs. SCE), cathodic and anodic Tafel slopes (β_c and β_a) and inhibition efficiency (IE%), calculated from Fig. 2, are given in Table 1. From Fig. 2, it can be observed that both cathodic and anodic current densities decrease in T3 presence, in the acidic solution. This result indicates the adsorption of the inhibitor molecules onto the active sites of the mild steel surface [23], and suggests that the inhibitor has influence on the anodic metal dissolution reaction, as well as on the cathodic reaction of hydrogen evolution [24]. It can also be observed that a successive increase in the inhibitor concentration resulted in a more pronounced inhibition behavior. The inhibition behavior could be attributed to the nitrogen atoms of the imidazole ring and the sulphur atom present in the alkyl chain of the inhibitor molecule.

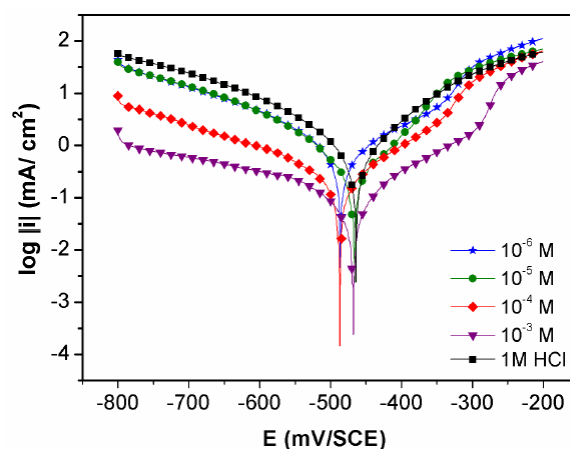


Figure 2. Polarization curves for mild steel in 1 M HCl containing different T3 concentrations.

In the inhibitors presence, both anodic and cathodic Tafel slopes remained almost unchanged (Fig. 2), indicating that the inhibitors acted by merely blocking the reaction sites of the metal surface, without changing the anodic and cathodic reaction mechanisms [25]. Furthermore, even in the inhibitor presence, it was observed that the corrosion rate increased at more positive potentials to ~ -0.250 V, and that the mechanism of anodic dissolution reaction changed. This behaviour may arise from a significant iron dissolution, leading to the inhibitor film desorption from the metal surface; the potential value can be defined as the “desorption potential” [23-24].

Table 1. Polarization parameters and corresponding inhibition efficiency for the corrosion of mild steel in 1 M HCl containing different concentrations of T3 at 308 K.

Concentration mol/L	E_{corr} (mV/SCE)	I_{corr} ($\mu\text{A cm}^{-2}$)	$-\beta_c$ (mV dec $^{-1}$)	β_a (mV dec $^{-1}$)	IE (%)
1M HCl	-464	2102	220	98	-
10^{-6}	-471	532	148	105	74.7
10^{-5}	-444	228	175	94	89.1
10^{-4}	-480	201	173	92	90.4
10^{-3}	-466	157	196	88	92.3

The inhibitor presence resulted in a slight shift of the corrosion potential towards the active direction, in comparison to the result obtained in the inhibitor absence. However, no significant shift of potential was observed in either anodic or cathodic direction, with respect to E_{corr} . This suggests that the investigated inhibitor exhibits a mixed-type behavior. The highest inhibition efficiency reached a maximum value of 92.3% at optimum T3 concentration (10^{-3} M). The efficiency was widely increased in T3 (92.3%) at 8 carbon chain, compared to T1 having 14 carbon chain (78%) [13]. The carbon chain influence is largely discussed in literature [8, 26-28].

Electrochemical impedance measurements

The electrochemical impedance spectroscopy (EIS) is a non-destructive technique that allows the evaluation of organic-coated metal surfaces in a rapid and convenient manner. Therefore, it is used to investigate the protective properties of organic corrosion inhibitors [28]. The obtained impedance spectra for mild steel in 1 M HCl, in the absence and presence of various T3 concentrations, were similar in shape, and are given in Fig. 3.

All semicircles correspond to a capacitive loop. The semicircles size depends on the additives concentration. The capacitive loop diameter increases with higher T3 concentrations. The occurrence of single, slightly depressed semicircle loops indicates a single time constant. This shows that the electrochemical process is charge transfer controlled, and that the electrode/electrolyte interface has a non-ideal capacitive behavior [29-30].

The Nyquist plots represented in Fig. 3 were analyzed by best fitting to the equivalent circuit model shown in Fig. 4, and the symbols values of this circuit are listed in Table 2. These parameters can be defined according to the following

convention: R_s is the solution resistance, R_p is the polarization resistance which contains the charge transfer resistance (R_{ct}) and the film resistance (R_f), and Q is the constant phase element (CPE) [31].

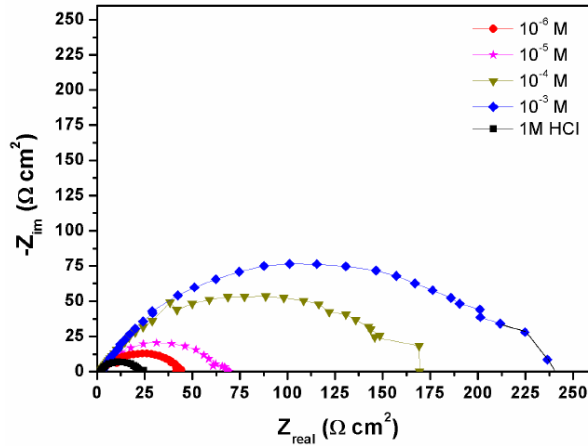


Figure 3. Nyquist diagrams for mild steel in 1 M HCl containing different T3 concentrations.

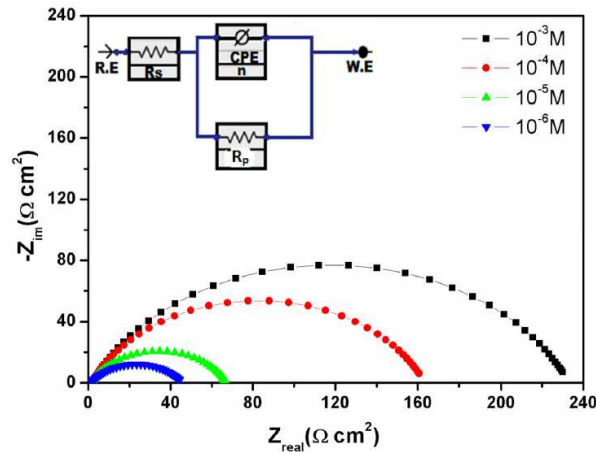


Figure 4. Fitted Nyquist plots; the inset shows the electrical equivalent circuit used for modeling the metal/solution interface in the inhibitor absence and presence.

Conventionally, in a Nyquist plot, the difference between the Z_{real} values at the highest and lowest frequencies is termed as the charge transfer resistance (R_{ct}). However, in the case of a metal surface immersed in a corrosive medium in the inhibitor presence, the contribution of the film resistance (R_f), diffuse layer resistance (R_d) and of the resistance due to other adsorbed species (R_a) cannot be neglected. Hence, in this case, we have used the term R_p , i.e., polarization resistance, to model the overall resistance contribution. The same equivalent circuit was proposed in the literature for carbon steel acidic corrosion in quinoxaline presence [32]. The use of CPE-type impedance has been extensively stated by previous reports [33-34]. CPE impedance is described as [35]:

$$Z_{CPE} = A^{-1}(j\omega)^{-n} \quad (3)$$

where A is the CPE constant (in $\Omega^{-1}\text{Sn cm}^{-2}$), E is the sine wave modulation angular frequency (rad^{-1}), $i^2 = -1$ is the imaginary number, and α is an empirical exponent ($0 \leq n \leq 1$), which measures the deviation from ideal capacitive behavior [36]. The impedance parameters obtained by fitting the EIS data to the equivalent circuit are listed in Table 2. The inhibition efficiencies at different inhibitor concentrations were calculated using equation 2.

Table 2. Impedance parameters for mild steel corrosion in 1 M HCl, in the absence and presence of different T3 concentrations.

	Conc (M)	R_s ($\Omega \text{ cm}^2$)	R_p ($\Omega \text{ cm}^2$)	$10^{-4}Q$ ($\Omega^{-1}\text{cm}^{-2}\text{s}^{-n}$)	n	C_{dl} ($\mu\text{F cm}^{-2}$)	IE (%)
1 M HCl	00	1.28 ± 0.01	23.26 ± 0.15	3.49 ± 0.07	0.80 ± 0.003	149.37	-
	10^{-6}	1.27 ± 0.02	41.38 ± 0.61	0.1 ± 0.01	0.66 ± 0.05	130.17	43.2
	10^{-5}	1.36 ± 0.02	66.9 ± 0.51	0.07 ± 0.05	0.71 ± 0.05	100.71	65.3
T3	10^{-4}	1.73 ± 0.03	162.8 ± 0.53	0.05 ± 0.07	0.74 ± 0.05	77.10	86.2
	10^{-3}	2.18 ± 0.02	230.9 ± 0.5	0.02 ± 0.04	0.74 ± 0.05	68.62	90.1

From Table 2, it can be observed that an increase in the inhibitors concentration causes an increase in R_p values, and a concomitant decrease in C_{dl} . This results from the increase in the surface coverage by the inhibitor, leading to an increase in IE %. The inhibitor protective layer thickness (δ_{org}) can be related to C_{dl} as follows:

$$C_{dl} = \frac{\epsilon_0 \epsilon_r}{\delta_{org}} \quad (4)$$

where ϵ_0 is the vacuum dielectric constant and ϵ_r is the relative dielectric constant. The decrease in C_{dl} values might result from the local dielectric constant lowering, or from an increase in the electrical double layer thickness, suggesting that the inhibitor molecules function by adsorbing at the metal/solution interface [36]. Thus, the observed decrease in C_{dl} values is caused by a gradual replacement of the water molecules by the inhibitor molecules adsorption onto the metal surface, which decreases the metal dissolution.

The potential of zero charge

In order to elucidate the adsorption mechanism, the surface charge on the mild steel surface is one of the governing factors. The surface charge of a metal can be determined by comparing the open circuit potential with the potential of zero charge (PZC). EIS measurements were used to evaluate the mild steel surface PZC in 1 M HCl, in the presence of 10^{-3} M of T3. A plot of C_{dl} values at each applied potential is shown in Fig. 5, forming a parabola with a minimum at -484 mV/SCE, which can be called the mild steel surface's PZC. In HCl, T3 exists as a moiety of benzimidazole cationic forms and chloride ions [37].

The mild steel OCP in the same conditions is -466 mV. The difference between OCP and PZC, which is Antropov's rational corrosion potential (Φ) = $E_{OCP} - E_{PZC}$, is 18 mV, which means that the metal surface is positively charged at the open circuit potential, in the present case.

The metal surface is positively charged with respect to PZC, but it becomes negatively charged, because the chloride ions will get adsorbed onto the metal surface. Now, the adsorbed Cl^- ions will attract benzimidazole cationic forms and protonated water molecules. Moreover, the excess positive charge on the electrode surface increases as more inhibitor molecules are adsorbed onto it [29].

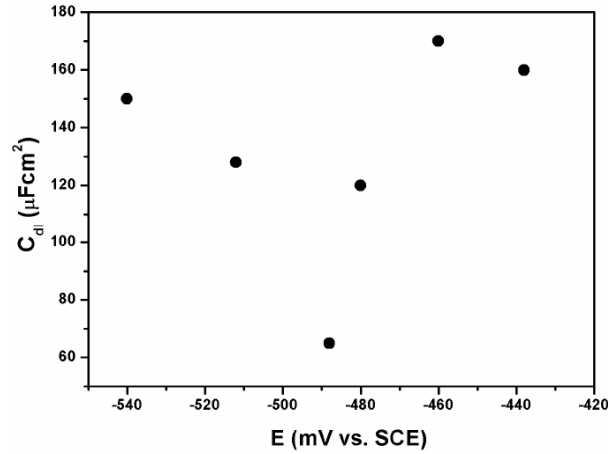


Figure 5. Plot of C_{dl} vs. applied electrode potential (E , mV/SCE) in 1 M HCl containing 10^{-3} M T3.

The displacement of water molecules from the metallic surface was largely discussed in several ways by Bockris et al. [38], according to the following reaction:



where x is the size ratio, that is, the number of water molecules replaced by one inhibitor molecule.

Adsorption isotherm

Basic information on the interaction between the inhibitor and the mild steel surface can be provided by the adsorption isotherm. In order to obtain the isotherm, a linear relation between the degree of surface coverage (θ) and the inhibitor concentration (C) must be found. Attempts were made to fit the θ values to various isotherms, including Langmuir, Temkin, Frumkin, etc. By far, the best fit was obtained with the Langmuir isotherm. The Langmuir isotherm is based on the assumption that all adsorption sites are equivalent, and that the particle binding occurs independently from nearby sites, whether occupied or not. According to this isotherm, θ is related to C by:

$$\frac{C}{\theta} = \frac{1}{K_{ads}} + C \quad (6)$$

where K_{ads} is the adsorption constant, C is the inhibitor concentration, and the surface coverage values (θ) are obtained from the EIS measurements for various concentrations. Fig. 6 shows the plots of C/θ against the inhibitor concentration

(C) at 308 K, and the expected linear relationship was obtained for this compound, with an excellent correlation coefficient ($R^2=0.99993$), confirming the validity of this approach. The slope of the straight line is unity, suggesting that the adsorbed inhibitor molecules formed a monolayer on the carbon steel surface, and that there was no interaction among the adsorbed inhibitor molecules. The obtained value of K_{ads} is 133226.8 M^{-1} , and it facilitates the determination of the standard free energy of adsorption (ΔG_{ads}°) by this equation:

$$\Delta G_{ads}^{\circ} = -RT \ln(55.5 K_{ads}) \quad (7)$$

where R is the gas constant, T is the absolute temperature of the experiment, and the constant value of 55.5 is the water concentration in a solution, in mol L^{-1} .

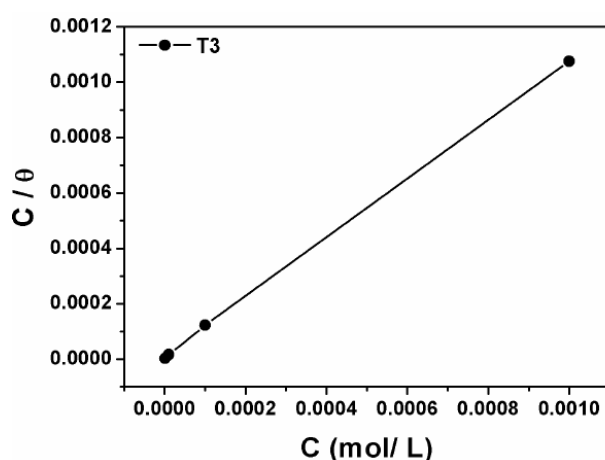


Figure 6. Langmuir isotherm of T3 on C-steel in HCl media.

The negative value (-40.5 kJ/mol) of ΔG_{ads}° , calculated from Eq. 7, indicates the spontaneity of the adsorption process, and the stability of the adsorbed layer onto the carbon steel surface. This value is widely discussed in literature, and is associated to chemisorption, as a result of the sharing or transfer of electrons from organic molecules to the metal surface, to form a coordinate bond [39].

Surface morphology

From the scanning electron microscopy (SEM) images shown in Fig. 7, a number of spots can be observed on the mild steel surface, arising due to the aggressive medium attack. However, in the T3 inhibitor presence, we can see a significantly smooth morphology, caused by the compound interaction with the metal surface's active sites. This results in an enhanced surface coverage of T3 molecules on the metal, so that there is a decrease in the contact between the metal surface and the aggressive medium.

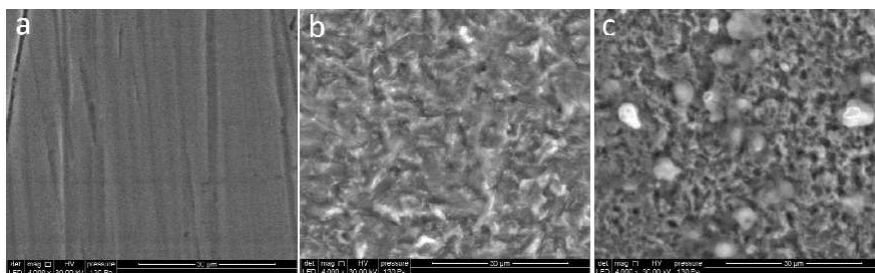


Figure 7. SEM micrographs of mild steel (a) polished, (b) after immersion in 1 M HCl without inhibitors, (c) after 6 h immersion in a 1 M HCl solution containing 10^{-3} M of T3.

Molecular dynamics simulations; adsorption energy calculations

In the current study, the dynamics simulation was carried out using the DMol³ code of Materials Studio 8.0 software from Accelrys Inc. USA [19]. For the DMol³ calculations, we chose the generalized gradient corrected B3LYP (Becke three parameters, Lee-Yang-Parr) functional and dual digital-based set with polarization functions on hydrogen's (DNP). This approach is shown to yield favorable geometries for a wide variety of systems.

The adsorption of a single inhibitor molecule, namely, 1-octyl-2-(octylthio)-1H-benzimidazole (T3), onto the iron surface, and the formation of the Fe-inhibitor (T3) complex occurred through molecular dynamics (MD) simulation, in an attempt to understand the interactions for the Fe (111)/T3/30 H₂O system. The calculation parameters used for the geometry optimization, via the module Forcite, are depicted in Table 3.

Table 3. The calculation parameters used in the geometry optimization for the T3-Fe-water system.

Champ of force	COMPASS
Convergence tolerance	Energy : 2.0×10^{-5} kcal/mol Force : 0.001 kcal/mol/Å Displacement : 1.0×10^{-5} Å Max Iterations : 500
Charges	Force field assigned
Quality	Ultrafine
Summation method	Electrostatic: group based Van der Waals : atom based

For the whole simulation procedure, the COMPASS (Condensed-phase Optimized Molecular Potentials for Atomistic Simulation Studies) force field [25] was used to optimize the structures of all the system's components. COMPASS is the first ab-initio force field that enables accurate and simultaneous prediction of chemical properties (structural, vibrational, conformational, etc.) and condensed-phase properties (equation of state, cohesive energies, etc.) for a broad range of chemical systems. It is also the first high quality force-field to consolidate parameters of organic and inorganic materials.

In the current study, the MD simulation was performed to study the system behavior, i.e., single inhibitor molecule / solvent molecules / iron surface [25].

Using the adsorption locator and the Forcite code implemented in the Materials Studio 8.0 [19], the single T3-molecule on Fe (111) configuration was sampled from a canonical ensemble. Fig. 8 shows the optimization energy curves of the inhibitor (T3) in the neutral form, and before putting it on the iron surface.

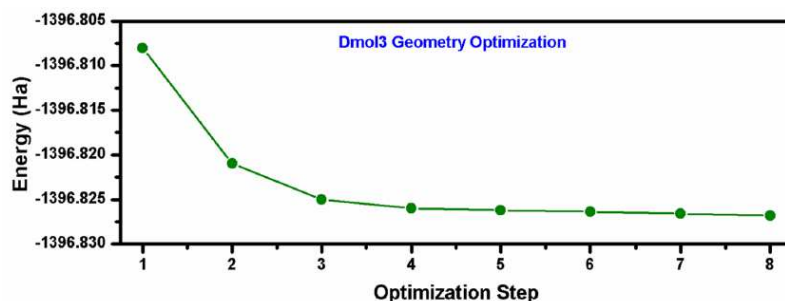


Figure 8. Optimization energy curves of the neutral form, before putting it on the iron surface.

In the canonical ensemble, the loading of imidazole derivatives on the iron (111) surface, as well as the temperature, are fixed. The adsorption energy distribution for the T3 /Fe (1 1 1)/30 H₂O complex system is presented in Fig. 9.

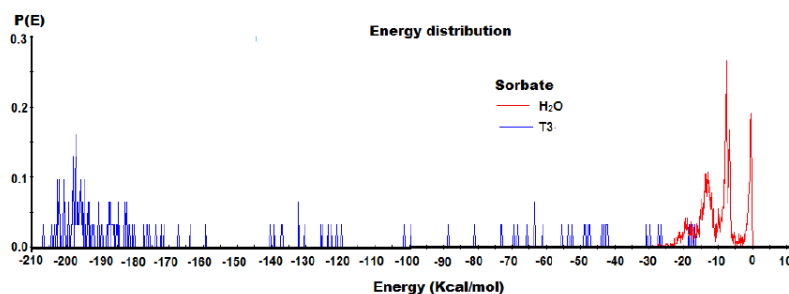


Figure 9. Adsorption energy distribution of the T3/30H₂O/ Fe (111) system.

Total energy, van der Waals energy, average total energy, electrostatic energy and intermolecular energy for the Fe (111) / T3 /30 H₂O system were calculated by optimizing the whole system, and are given in Fig. 10.

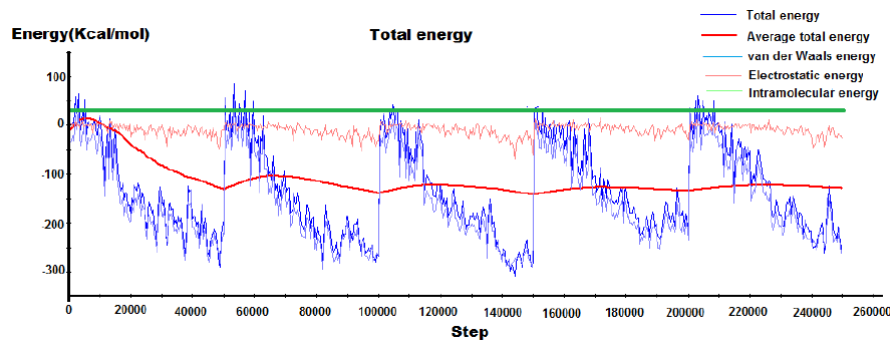


Figure 10. Total energy distribution for the Fe (111)/T3/30H₂O complex during the energy optimization process.

The most stable low-coverage structures of the single inhibitor molecule (T3) on the Fe (111)/30H₂O system, using Monte Carlo simulations, are depicted in Fig. 11, and the adsorption energies for the T3-Fe_{ads} complex are shown in the side and top views of the stable adsorption configurations.

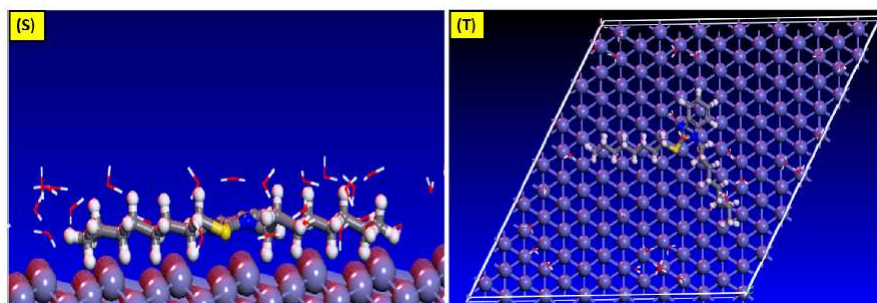


Figure 11. Side (S) and top (T) views of stable adsorption configurations for the Fe (111)/T3/30 H₂O system, obtained using the Monte Carlo simulations.

An inspection of Fig. 11 shows that the adsorption centers on the iron (111) surface are nitrogen, sulfur and the π -electron system, and that the form of the neutral T3 inhibitor interacts in a parallel way with the iron (111) surface (Fe-S-C=N: -79.496° , Fe-N-C-C: -76.99° , Fe-N=C-N: 123.273° and Fe-S-C=N: 80.33°). The measured shortest bond distances between the closest heteroatoms (-S- & -N=) of T3 and the iron (111) surface at equilibrium were as follows: T3-Fe interactions: ($d_{\text{Fe-S}}$: 2.909\AA , $d_{\text{Fe-N}}$: 2.604\AA , $d_{\text{Fe-N}}$: 3.934\AA). A shorter bond distance implies stronger interactions (high inhibition efficiency) [40]. The strong bonding of T3 heteroatoms with the Fe atom ensures the chemical nature of the adsorption process (chemisorption). This indicates that T3 is an efficient inhibitor. The values for the outputs and descriptors calculated by the Monte Carlo simulation for the Fe (111)/T3/30 H₂O system are listed in Table 4.

Table 4. Outputs and descriptors for the lowest adsorption configurations for the Fe (111)/T3/ 30 H₂O system, calculated by the Monte Carlo simulation (all in Hartree).

System	E_{Total}	E_{ads}	R.A.E.	D_{Energy}	$\frac{dE_{\text{ads}}}{dN_{\text{i}}}$ T3	$\frac{dE_{\text{ads}}}{dN_{\text{i}}}$ H ₂ O
Fe (1 1 1)/T3/30 H ₂ O	-0.729	-0.780	-0.7851	0.0045	-0.316	-0.00053

The parameters presented in Table 4 include total energy (E_{Total}) in Hartree, of the substrate-adsorbate configuration. The total energy is defined as the sum of the energies of the adsorbate components. In addition, adsorption energy (E_{ads}) reports the energy released (or required) when the T3 relaxed adsorbate components are adsorbed onto the substrate. The adsorption energy is defined as the sum of the rigid adsorption energy (R.A.E) and the deformation energy for the adsorbate components. The rigid adsorption energy reports the energy released (or required) when the unrelaxed T3 molecule, before the geometry optimization step, is adsorbed onto the iron (111) surface, in the presence of 30 water molecules. The deformation energy (D_{Energy}) reports the energy released when the adsorbed T3 molecule is relaxed on the iron surface. Table 4 also

shows dE_{ads}/dN_i , which reports the energy of Fe–T3 configurations where one of the T3 molecules has been removed.

It is quite clear from Table 4 that the adsorption energy value is negative (-0.780 Hartree), which denotes that the adsorption could spontaneously occur. The large negative value indicates that the T3-Fe_{ads} organometallic complex is the most stable, and leads to stronger adsorption [41]. The T3 adsorption energy value (-0.316 Ha) is far higher than that of the water molecules (-0.00053 Ha). This indicates the possibility of a progressive replacement of the water molecules from the iron surface, leading to the formation of a stable layer that can protect the metal surface against aqueous corrosion.

Conclusions

In summary, a new 2-mercaptobenzimidazole derivative (T3) was synthesized, characterized, and thereafter investigated as a corrosion inhibitor for C-steel in 1 M HCl. Electrochemical (potentiodynamic polarization and EIS) methods were used for corrosion testing. T3 acted as an efficient inhibitor (92% at 10^{-3} M), and exhibited a mixed type behavior. Fitted EIS curves ensured the adsorption phenomenon, and MD simulation provided more details. The results of surface morphology, before and after corrosion, corroborate electrochemical tests observations.

References

1. Puthalath R, Surendranathan AO, Murthy ChSN. J Mater Environ Sci. 2012;3:856-869.
2. Finšgar M, Jackson J. Corros Sci. 2014;86:17-41.
3. Ghazouni A, Benchat N, El-Hajjaji F, et al. J Alloys Compd. 2016;693:510-517.
4. Chauhan DS, Ansari KR, Sorour AA, et al. Int J Biol Macromol. 2018;117:1747-1757.
5. El-Hajjaji F, Messali M, Aljuhani A, et al. J Mol Liq. 2018;249:997–1008.
6. El Ouali A, Chetouani A, Hammouti B, et al. Port Electrochim Acta. 2013;31:53-78.
7. Louadi YE, Abridach F, Bouyanzer A, et al. Port Electrochim Acta. 2017;35:159-168.
8. Touhami F, Kertit S, Hammouti B, et al. Ann Chim Sci Mat. 1999;24:581-586.
9. Khaled KF. Electrochim Acta. 2003;48:2493-2503.
10. El Aoufir Y, El Bakri Y, Lgaz H, et al. J Mater Environ Sci. 2017;8:3290-3302.
11. Benabdellah M, Tounsi A, Khaled KF, et al. Arab J Chem. 2011;4:17-24.
12. Abboud Y, Abourriche A, Saffaj T, et al. Appl Surf Sci. 2006;252:8178-8184.
13. El Ouasif L, Merimi I, Zarrok H, et al. J Mater Environ Sci. 2016;7:2718-2730.

14. Metropolis N, Rosenbluth AW, Rosenbluth MN, et al. J Chem Phys. 1953;21:1087-1093.
15. Delley B. J Chem Phys. 1990;92:508-517.
16. Delley B. J Chem Phys. 2000;113:7756-7764.
17. Frenkel D, Smit B. Understanding Molecular Simulation: From Algorithms to Applications. 2nd ed. San Diego: Academic Press; 2002.
18. Kirkpatrick S, Gelatt CD, Vecchi MP. Science. 1983;220:671-680.
19. Materials Studio v 8.0.100.21. San Diego: Accelrys Software Inc; 2014.
20. San-Miguel MA, Rodger PM. J Mol Str (Theochem). 2000;506:263-272.
21. Sun H. J Phys Chem B. 1998;102:7338-7364.
22. Sun H, Ren P, Fried JR. Comput Theor Polymer Sci. 1998;8:229-246.
23. Solmaz R. Corros Sci. 2010;52:3321-3330.
24. Behpour M, Ghoreishi SM, Soltani N, et al. Corros Sci. 2009;51:1073-1082.
25. Galai M, El Faydy M, El Kacimi Y, et al. Port Electrochim Acta. 2017;35: 233-251.
26. Herrag L, Hammouti B, Aouniti A, et al. Acta Chim Slov. 2007;54:419-423
27. Sankarapapavinasan S, Pishapinadon F, Ahmed MF. Corros Sci. 1991;32:193-203.
28. TrabANELLI G, Zucchi F, Gullini G, et al. Werkst Korros. 1968;20:407-411.
29. Zarrok H, Oudda H, El Midaoui A, et al. Res Chem Interm. 2008;38:2051-2063.
30. Mahato N, Singh MM. Port Electrochim Acta. 2011;29:233-251.
31. Kissi M, Bouklah M, Hammouti B, et al. Appl Surf Sci. 2006;252:4190-4197.
32. Aoun SB, Bouklah M, Khaled KF, Hammouti B, et al. Int J Electrochem Sci. 2016;11:7343-7358.
33. Zarrouk A, Zarrok H, Ramil Y, et al. J Mol Liq. 2016;222:239-252.
34. Popova A, Christov M. Corros Sci. 2006;48:3208-3221.
35. Popova A, Christov M, Vasilev A. Corros Sci. 2007;49:3290-3302.
36. Singh P, Chauhan DS, Srivastava K, et al. Int J Ind Chem. 2017;8: 363-372.
37. Singh UP, Maurya R, Kashyap S. Struct Chem. 2014;25:733-743.
38. Bockris JO'M, Reddy AKN, Gamboa-Aldeco M. Modern Electrochemistry. vol 24. Fundamentals of Electrodeics. New York: Kluwer Academic Publ; 2002.
39. Zarrok H, Zarrouk A, Salghi R, et al. Int J Electrochem Sci. 2013;8:11474-11491.
40. El-Hajjaji F, Belkhmima RA, Zerga B, et al. Int J Electrochem Sci. 2014;9:4721-4731.
41. Singh A, Ebenso EE, Quraishi MA. Int J Electrochem Sci. 2012;7:4766-4779.